INKJET-PRINTED HIGHLY TRANSPARENT SOLAR CELL ANTENNAS

by

Jesus A. Arellano

A thesis submitted in partial fulfillment
of the requirements for the degree

of

MASTER OF SCIENCE

in

Electrical Engineering

Approved:

Dr. Reyhan Baktur Major Professor	Dr. Edmund Spencer Committee Member
Dr. Jacob Gunther Committee Member	Dr. Mark R. McLellan Vice President for Research and Dean of the School of Graduate Studies

UTAH STATE UNIVERSITY
Logan, Utah

2011

Abstract

Inkjet-Printed Highly Transparent Solar Cell Antennas

by

Jesus A. Arellano, Master of Science

Utah State University, 2011

Major Professor: Dr. Reyhan Baktur
Department: Electrical and Computer Engineering

Small satellites, especially Cube Satellites (CubeSats), have become important vehicles for space exploration. One of the challenges CubeSats face is limited surface area. This limitation poses a question for antenna design–where to mount the antenna? This thesis presents a study where the antennas are directly integrated on top of solar cells. In order to achieve such integration, the antennas have to be highly transparent to light. This thesis aims at the transparency of 95%. Methods to effectively generate transparent antenna by using inkjet printing are discussed in detail and interaction between solar cells and antennas have been assessed and presented. It is found that the presence of solar cells cast a degree of gain reduction of the antenna, but such a loss may be improved with a more precise integration and by increasing the operational frequency. The effect of the antenna on solar cell performance is concluded to be less than 3%, promising a feasibility of implementing highly transparent antennas on CubeSats.

(62 pages)

Public Abstract

Inkjet-Printed Highly Transparent Solar Cell Antennas

by

Jesus A. Arellano, Master of Science

Utah State University, 2011

Major Professor: Dr. Reyhan Baktur
Department: Electrical and Computer Engineering

Small satellites, especially Cube Satellites (CubeSats), have become important vehicles for space exploration. One of the challenges CubeSats face is limited surface area. This limitation poses a question for antenna design–where to mount the antenna? Transparent antenna is a solution to resolve the competition between solar cells and antennas for surface area. The transparent antennas can be directly integrated on top of solar cells without requiring additional space. It is for this reason that this thesis focuses on the integration of highly transparent meshed antenna with solar cells. Even though transparent antennas allow light to travel light through them, they do repel a small portion of total amount. It is important to consider that solar cells need a significant amount of solar light in order to work properly. It is for this reason that a transparency of 95% becomes one of the main aims of this study. This thesis explores different prototyping methods to achieve highly transparent and effective meshed patch antennas. Considering the trade-offs between three fabrication schemes (electroformation, screen printing, and inkjet printing), the inkjet printing method is chosen to be the prototyping method. The inkjet printing method is the economical of all methods given the reduced amount of materials needed. Conductive ink (Nanosilver aqueous dispersive ink Metalon JS-B25P), receptive PET film (Novele IJ-220), and a commercial inkjet printer (less than $100.00) are the only materials needed. The

printing routine and curing techniques are discussed in detail as part of this thesis. After achieving highly transparent ($\geq 95\%$) antennas, the next task is to integrate them on top of triple junction space-certified solar cells. There are two main objectives in initial integration: (1) to assess the effect of solar cells on the antenna's performance, and (2) to assess the effect of the antennas on solar cell's performance. In order to achieve the first objective, several different antennas (solid non-transparent patches and meshed transparent patches) were tested on substrates (solar cell cover glass) with and without solar cells embedded. In order to achieve the second objective, a meshed patch antenna with 95% transparency and without the feed-line is placed on an active solar panel. The efficiency of the solar panel was then measured using standard procedure at SDL (Space Dynamics Laboratory, Logan UT). It is found that the presence of solar cells cast a degree of gain reduction of the antenna, but such a loss may be improved with a more precise integration and by increasing the operational frequency. The effect of the antenna on solar cell performance is concluded to be less than 3%, promising a feasibility of implementing highly transparent antennas on CubeSats.

To my beloved parents and sister

Acknowledgments

I would like to express my profound appreciation to my advisory committee: Dr. Edmund Spencer, Dr. Jacob Gunther, and most especially to my major advisor, Dr. Reyhan Baktur. I am thankful for the opportunity to be part of the printed antennas research. Special thanks to Dr. Reyhan Baktur for her time, patience, and understanding. It has been a real honor to work with her.

My gratitude also goes to Dave Pope and Ian Rawson at Novacentrix Corp. for the time they took to answer all my questions concerning conductive inks and printing methods. I would like to also thank the staff of the Electrical Engineering store at Utah State University. Special thanks to Heidi Harper for her readiness to help and make sure I always had all the implements needed to keep moving forward.

This thesis was funded by National Science Foundation through the award #0801426.

Jesus A. Arellano

Contents

Page

Abstract . . . . . **iii**

Public Abstract . . . . . **iv**

Acknowledgments . . . . . **vii**

List of Tables . . . . . **ix**

List of Figures . . . . . **x**

1 Introduction **1**
1.1 Optically Transparent Antennas 1
1.2 Transparent Conductors 1
1.3 Meshed Patch Antennas 2
1.4 Integrated Optically High Transparent Antennas 2

2 Design of Highly Transparent Antenna **4**
2.1 Optical Transparency 4
2.2 Transparency, Efficiency, and Gain 5
2.3 Silver, Copper, and PEC Meshed Patches 7
2.4 Substrates 8

3 Fabrication Method **9**
3.1 Electroformed Mesh 9
3.2 Screen Printing 9
3.3 Inkjet Printing 10
3.4 Inkjet Printing Method Used at USU 11
3.4.1 Pre-Printing Routine 12
3.4.2 Printing Routine 13
3.4.3 Post-Printing and Curing Routine 14

4 Extensive Measurements **17**
4.1 Meshed and Solid Patch Antennas 17
4.2 Orientation of the Antenna on Solar Cells 20
4.3 Effect of Solar Cells on Antenna Gain 27
4.4 Discussions on Gain Enhancement 41
4.5 Discussions on Skin Depth 42
4.6 Effect of the Transparent Antennas on Solar Cell Performance 44

5 Conclusions **46**

References **48**

List of Tables

Table Page

2.1 PEC, silver, and copper solid patch antennas. 8

4.1 S11 and gain of meshed patch antennas on Rogers board. 18

4.2 Measurement 8. 23

4.3 Measurement 9. 25

4.4 Measurement 10. 28

4.5 Measurement 11. 29

4.6 Measurement 12. 30

4.7 Measurement 13. 31

4.8 Measurement 14. 32

4.9 Measurement 15. 33

4.10 Measurement 16. 34

4.11 Measurement 17. 35

4.12 Measurement 18. 36

4.13 Measurement 19. 37

4.14 Measurement 20. 38

4.15 Measurement 21. 39

4.16 S11 and gain of meshed patch antennas on plastic and gel. 41

4.17 Gain difference for antennas on plastic and gel. 41

4.18 Calculated skin depth. 43

List of Figures

Figure Page

2.1 Geometry of meshed patch antenna. 5

2.2 Gain vs transparency. 6

2.3 Efficiency vs transparency. 6

2.4 Gain vs transparency. 7

3.1 Priming of cartridges. 13

3.2 Printing. 14

3.3 Curing of antennas. 14

3.4 Baked printout line. 15

3.5 Air dried printout line. 15

3.6 Cleaning of printer. 16

4.1 S11 for measurement 2. 18

4.2 E plane radiation pattern for measurement 2. 18

4.3 S11 for measurement 3. 19

4.4 E plane radiation pattern for measurement 3. 19

4.5 S11 for measurement 5. 19

4.6 E plane radiation pattern for measurement 5. 20

4.7 CV-2500 controlled volatility silicone. 21

4.8 Perpendicular orientation. 22

4.9 Parallel orientation. 22

4.10 S11 of parallel setup. 23

4.11 S11 of vertical setup. 24

4.12 E plane radiation pattern for parallel setup. 24

4.13 E plane radiation pattern for vertical setup. 24

4.14 S11 of parallel setup. 25

4.15 S11 of vertical setup. 25

4.16 E plane radiation pattern for parallel setup. 26

4.17 E plane radiation pattern for vertical setup. 26

4.18 S11 for shielded board - Measurement 10. 28

4.19 E plane radiation pattern for vertical setup - Measurement 10. 28

4.20 S11 for shielded board - Measurement 11. 29

4.21 E plane radiation pattern for vertical setup - Measurement 11. 29

4.22 S11 for shielded board - Measurement 12. 30

4.23 E plane radiation pattern for vertical setup - Measurement 12. 30

4.24 S11 for unshielded board - Measurement 13. 31

4.25 E plane radiation pattern for vertical setup - Measurement 13. 31

4.26 S11 for unshielded board - Measurement 14. 32

4.27 E plane radiation pattern for vertical setup - Measurement 14. 32

4.28 S11 for shielded board - Measurement 15. 33

4.29 E plane radiation pattern for vertical setup - Measurement 15. 33

4.30 S11 for shielded board - Measurement 16. 34

4.31 E plane radiation pattern for vertical setup - Measurement 16. 34

4.32 S11 for shielded board - Measurement 17. 35

4.33 E plane radiation pattern for vertical setup - Measurement 17. 35

4.34 S11 for shielded board - Measurement 18. 36

4.35 E plane radiation pattern for vertical setup - Measurement 18. 36

4.36 S11 for unshielded board - Measurement 19. 37

4.37 E plane radiation pattern for vertical setup - Measurement 19. 37

4.38 S11 for unshielded board - Measurement 20. 38

4.39 E plane radiation pattern for vertical setup - Measurement 20. 38

4.40 S11 for unshielded board - Measurement 21. 39

4.41 E plane radiation pattern for vertical setup - Measurement 21. 39

4.42 SDL setup. 45

Chapter 1

Introduction

1.1 Optically Transparent Antennas

The application of optically transparent antennas is increasing and extending to more fields of application. These fields of application now range from vehicular communications and navigation [1] to the integration of solar cells, and antennas in small satellites [2]. In the particular case of small satellites, there is an increasing need to condense their physical dimensions while maintaining optimal radiation properties. For instance, solar cells, antennas, and space instruments must be mounted on a limited amount of surface area. The challenge of this application is the need to integrate elements in order to more effectively use the available surface area. The antennas and solar cells must be situated in the same area without hindering the effectiveness of each other; it is for this reason that optically transparent antennas become a special interest. Various approaches have been considered to develop the most feasible course to construct transparent antennas. These include the construction of transparent antennas by using transparent conductors, the placing of patch antennas under solar cells [3], the creation of radiating slots on the ground under the solar cells [4], and finally the integration of optically transparent meshed patch antennas on top of off-the shelf solar cells [2].

1.2 Transparent Conductors

The use of transparent conductors has had different approaches, including transparent antennas that were constructed from thin sheets of clear polyester with an AgHT-8 optically transparent conductive coating [1]. A well-known example of a succesful conductor is Indium Tin Oxide (ITO), which belongs to the family of oxides and exhibits high optical transparency ($> 80\%$ at 550nm wavelength) at very thin depositions (100nm-1.2um) and

considerable electrical conductivity (aprox. 10^5 S/m) [5]. ITO has been used in the development of topical patch antennas [6, 7] that can likely be placed on solar cells. However, at very thin depositions, efficiency of patch antennas is intensely restricted by skin and ground effects [8].

1.3 Meshed Patch Antennas

The need for alternative methods to obtain optical transparency has motivated researchers to study meshed patch antennas [9–13]. According to "Meshed patch antennas integrated on solar cells" [2], the meshing of patch antennas does not compromise the radiation properties of it, and with an appropriate geometrical design it exhibits a similar behavior to solid patch antennas. This is a remarkable achievement given that microstrip antennas have been widely and confidently applied in various communications systems in the last decades [14]. Previous studies that have implemented the mesh patch designs have successfully reached transparency and efficiency values of 80% and 50%, respectively [2].

1.4 Integrated Optically High Transparent Antennas

Previous studies have explored the performance of different integrated transparent antennas desings. For instance, Vaccaro et al. have successfully developed slot antennas that have been integrated onto solar cells. This development allowed for a more efficient use of the available space for solar cells. Amorphous silicon solar cells were cut and grown on the surface of antennas exploring diverse applications. These solar antennas were able to function at their maximum capacity achieving gains of up to 30 dBi [15], given that no light going onto the solar panels was blocked. The present study explores a new integrated transparent antenna design. This new design consists of meshed patch antennas that will be placed on top of solar cells on the walls of small satellites. The covering of certain areas on the solar cells is unavoidable. In order to ensure the proper functioning of the solar cells, a minimum of 90% of the total surface area must be left uncovered [2]. It is under these circumstances that the construction of 95% optically transparent meshed patch antennas becomes the paramount target of the present study. Printed meshed patch antennas can

achieve these transparency levels due to their flexible design dimensions. The fabrication method of these printed antennas is significantly simple. The optimal transparency levels and accessible nature of the fabrication process make of the printed meshed patch antennas an idoneous solution to challenges previously mentioned.

Chapter 2

Design of Highly Transparent Antenna

2.1 Optical Transparency

This optical transparency is defined by the percentage of the see-through area of the patch antenna [16]. The geometry of the meshed patch antenna is shown in Fig. 2.1. The antenna is fed by a T-line, the width and lengths of the patch are represented by W and L, respectively. The distance between the edge of the patch and the head of the feed line is represented by G, and finally the height of the head of the feed line is represented by H. It will be shown later that these two parameters (G and H) are of particular importance at the time of finding a good matching point between the patch and the feed line; it will allow the necessary tuning to obtain resonating S11 parameter values. The transparency of the patch is calculated by the percentage of see-through area of the patch as represented below

$$P_{tran} = \frac{(A_{patch} - A_{metal})}{A_{patch}} \times 100\%. \tag{2.1}$$

A series of meshed patches have been simulated in HFSS (High frequency structure simulator) exhibiting different line dimensions and line densities to establish basic properties of gain, efficiency, line width, and resonant frequency. Initially line width values of 0.5mm were used for all lines within the patch for simulation purposes. Even though they showed acceptable S11 parameter values, the transparency reached with these line widths was extremely low considering that the purpose of the present study is to achieve a 95% transparency level. Another consideration is that the number of lines perpendicular to the length of the patch can be reduced given that they do not affect the performance of the antenna in a significant manner [2]. Under this same concept, the dimensions of these lines will be decreased with respect to the perpendicular lines in order to improve transparency.

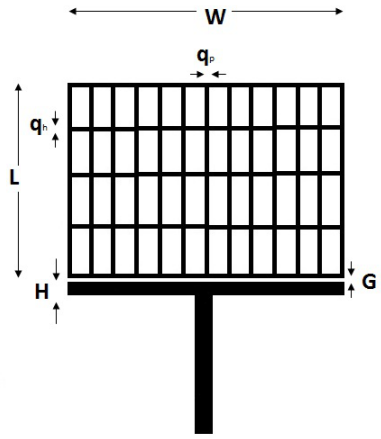

Fig. 2.1: Geometry of meshed patch antenna.

2.2 Transparency, Efficiency, and Gain

The antenna geometry, transparency, and gain are related. Turpin and Baktur have shown that when the width of the mesh line is fixed, the gain of the antenna decreases as transparency increases [2]. When the transparency is fixed, however, thinner linewidth gives better antenna performance [2]. In addition, the effect of perpendicular mesh lines (Fig. 2.1) is stronger on the antenna performance than the horizontal lines [2]. Based on the previous study, several simulation studies have been carried out. In the following studies, the width (q_p) of the perpendicular lines and the horizontal lines (q_h) were set to be 0.15 mm and 0.1 mm, respectively. The number of horizontal lines was kept the same, while the number of vertical lines was varied slightly to achieve different transparencies. Accordingly, the feed design is modified slightly by changing the value of G to achieve matching for each antenna design. The results of those studies were plotted in Fig. 2.2 and Fig. 2.3. These results are consistent with Turpin's study except for the antennas' very high transparency ($> 94\%$). It is seen that the feed design has an effect on antenna gain, and therefore adjusting the distance of the T-line (marked as G in Fig. 2.1) to achieve the highest gain for a given transparency is important. When 95% transparency is the target frequency, then one should reduce the line-width to achieve better gain. Otherwise, as seen from Fig. 2.2, there will be a significant reduction in gain when the transparency is increased without changing the width of mesh-lines.

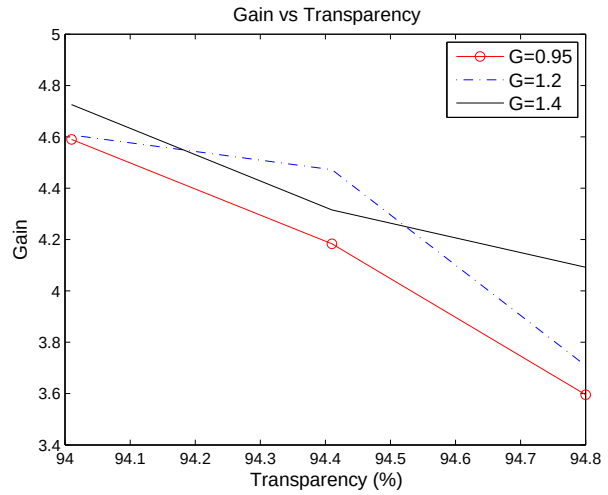

Fig. 2.2: Gain vs transparency.

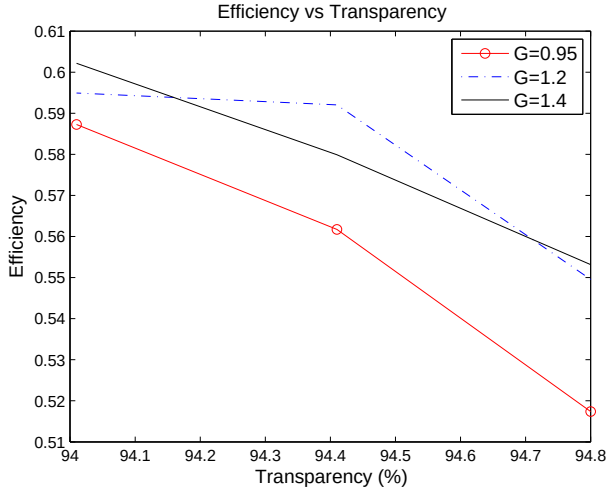

Fig. 2.3: Efficiency vs transparency.

2.3 Silver, Copper, and PEC Meshed Patches

In order to study the effect of the conductor on the meshed patch antennas, a simulation study was performed on meshed antennas designed from perfect electric conductor (PEC), silver, and copper. The results are plotted in Fig. 2.4. In this study, the width of the mesh lines were kept the same for all three types of antennas and the transparency was changed by changing the number of lines. Accordingly, the G value was modified in each design for good matching. As a comparison, three solid patch antennas designed from PEC, silver, and copper were studied. The gains of the solid patch antennas are listed in Table 2.1. It can be seen that for solid patch antennas, the effect of the material on the gain is small, which means the difference between a PEC patch and copper patch is trivial at our design frequency. However, for meshed antenna, there is a big difference in gain between PEC antenna and copper antenna. Therefore, due to meshing, a copper or silver meshed antenna has significant gain reduction compared to a PEC meshed antenna. It is also seen that a silver meshed antenna performs slightly better than a copper antenna, but the difference is small and one may choose copper mesh when price is considered.

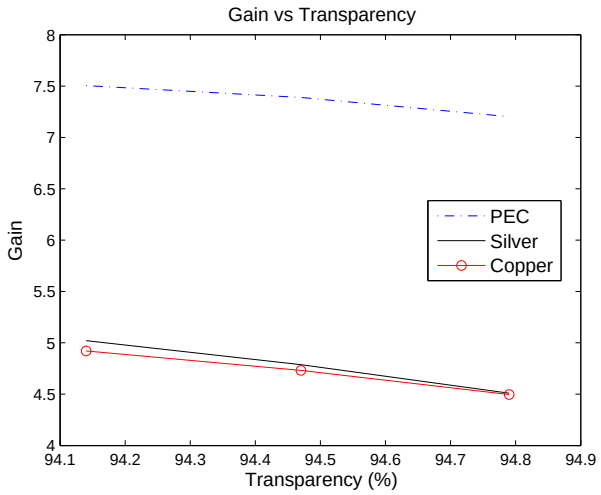

Fig. 2.4: Gain vs transparency.

Table 2.1: PEC, silver, and copper solid patch antennas.

Material	Res. Frequency	S11	Gain
PEC	2.51 Ghz	-17.70	7.67 dB
Silver	2.51 Ghz	-17.16 dB	7.46 dB
Copper	2.5 Ghz	-17.32 dB	7.43 dB

2.4 Substrates

In this thesis study, there are three types of substrates on which the meshed antennas have been prototyped. The first type is RT/duroid 5880 high frequency laminate. It has a permittivity value of 2.2 and a thickness equal to 0.787 mm [16]. The second type is RO 4003C high frequency laminate. It has a permittivity value of 3.38 and a thickness equal to 0.813 mm [16]. The third type is CV-2500 controlled Volatility Silicone. It has a permittivity value of 2.6 and a thickness equal to 1.005 mm [17].

Previous study has shown evidence that a substrate with lower permittivity will guarantee a better radiation performance. Also, it has been reported in the past that a thinner substrate results in a less efficient radiator [18]. This means that the thin cover glass of solar cell may yield a very low gain. Therefore, additional methods may be needed to improve the gain. A feasible gain improvement method is presented in Section 4.2 of this thesis.

Chapter 3

Fabrication Method

There are three well-established methods to prototype meshed patch antennas: designing antennas from electroformed meshes, screen printing, and inkjet printing.

3.1 Electroformed Mesh

Electroforming is a highly specialized metal forming process which electrodepositates metal in a plating bath over a base form or mandrel which is subsequently removed. The plating formed is much thicker than in the case of electroplating, and is capable of supporting itself after the mandrel is removed. This plating or coating formed becomes the final product. Simple and complex parts can be produced, with wall thickness as small 0.025mm. An important advantage of electroforming worth mentioning includes very high dimensional accuracy which is able to reproduce the external shape of the mandrel within one micrometer. Other advantages include repeatability of the process and good strength of the final product [19]. However, stripping the final product from the mandrel can be challenging and damage the formed geometry at times. A practical disadvantage of the off-the-shelf electroformed meshes to our study is the lack of flexibility in mesh geometry. As the mesh-line geometry (Section 2.2) is important to antenna gain and transparency, it is important to carefully design the mesh geometry to achieve an optimal antenna gain and transparency. For the off-the-shelf meshes, since the geometries are limited, the antenna transparency and gain are accordingly limited.

3.2 Screen Printing

This simple printing technique consists of the application of conductive ink into the open areas of a patterned mask that is held over a substrate sheet. The mask is then

removed and the substrate is baked at a relatively low temperature in order to evaporate the solvent present in the conductive ink. The baking process completely sets and solidifies the ink on the substrate after a few hours. Line widths of around 100 microns and thickness in the order of 10 microns are attainable through this process [20]. Although screen printing may result in thin lines with acceptable accuracy, especially with certain highly accurate printing process, in practice, the accuracy in line width and uniformity of lines are not high enough for printing highly transparent antennas. In addition, it is also limited to simple polygonal geometries and results in a considerable amount of wasted ink.

3.3 Inkjet Printing

Inkjet printing is a material-conserving deposition technique used for liquid inks which consist of solutes dissolved in solvents. This printing process comprises of the ejection of precise amounts of ink from ink filled chambers. These chambers house a piezoelectric material and are connected to nozzles. When a voltage is applied, the piezoelectric material changes shape, and the chamber is contracted. This reduction of the chamber volume sets up a shockwave and causes a liquid drop to be ejected from the nozzle [21]. The ejected drop then falls onto the substrate under the applied forces of gravity and air resistance. The spreading of the ink along the surface is governed by the momentum acquired throughout the motion and surface tension present on the surface of the substrate [22]. An experimental study on the spreading of inkjet printed droplets has shown that drop spreading and final printed shape depend on the viscosity or molar mass of the polymer [23]. The same group also detected the existence of relationships between dried droplet diameters and printing height at low and high polymer concentration [24]. The chamber can easily be refilled through the inlet ports by capillary action at the orifice; this allows a reduction of material wastage and a reduction of cost by enabling reusability of the equipment. Drop size limiting factors include the ink, the surface energy of the substrate, and the nozzle diameter. This last one is the fundamental lower bounding factor on the drop size and ultimately the line width. However, it is also important to mention that it is the nozzle that enables the system with depositing versatility [25].

In summary, the layer thickness control, repeatability of the process, low cost, reduction of material wastage, and scalability are attributes that make the Inkjet printing system the most idoneous fit to the requirements of the present study.

3.4 Inkjet Printing Method Used at USU

The antennas developed and fabricated in the present study have transparency values close to 95%. These values were achieved by first designing meshed patch antennas in HFSS and then developing a suitable printing system. This particular printing system consists of three important elements: printer, ink, and substrate. In order to obtain the desired accuracy and performance of all these elements, they must be symbiotically compatible with each other. The resolution of printed patterns depends greatly on the drop size and spot interspacing [26]. For this reason, the present inkjet printing setup is based on an Epson Stylus C88+printer. This printer uses the advantageous CMYK (Cyan, Magenta, Yellow, Black) drop-on-demand Micro Piezo ink jet technology, allowing a variable ink droplet size as small as 3 picoliters [27]. Another advantage that this printer offers is the wide variety of paper types that can be used. The ink-substrate interaction was specially monitored in order to assure the best curing conditions for the ink, and in that manner provide highly accurate printing quality. The printed electronics inkjet receptive substrate Novele IJ-220 and the Nanosilver aqueous dispersive ink Metalon JS-B25P were chosen. The IJ-220 is a PET-based substrate specifically engineered to be used in conjunction with Metalon conductive inks. This substrate's coating promotes the uniform deposition of the Metalon JS-B25P used in this printing system. This silver based ink is designed to produce circuits on treated polymer films such as the Novele IJ-220 coated PET. This ink presents a resistivity of 5 micro-ohms per centimeter when printed with the Epson Stylus C88+ and cured with the post-process Pulse Forge 3100 [28]. The JS-B25P has a silver content equal to 25 wt% and a viscosity of 5 cp making it the most suitable ink for the inkjet printer used in this printing system. Previous attempts to print antennas implemented the same Epson stylus C88+ printer used in the present study. The Metalon JS-015 and Metalon JS-011 Nanosilver inks used in prior studies were tested on inkjet photo paper with

no successful results. These inks generate the clogging of the printer's head, impede the continuous printing process and significantly decrease the levels of productions due to their viscosity. The printing quality is also affected exhibiting poor conductivity and radiation values. Even though the ink and substrate were replaced in the present study, a Metalon aqueous vehicle has been included. This cleaning solution was added to the printing system in order to ensure the complete cleaning of the printer's head after its use and the normal performance of the printer. The complete printing process includes the following steps.

3.4.1 Pre-Printing Routine

First, in order for the printer to be initialized the Epson OEM (Original equipment manufacturer) cartridges must be installed. Next, a nozzle check must be performed in order to ensure the proper firing of all nozzles. Head cleaning is required when the nozzle check is faulty; this process is to be repeated until the nozzle check is satisfactory. Following the nozzle check, empty CMYK replacement cartridges are filled with the Metalon aqueous vehicle cleaning solution. These cartridges have to go through a priming process before use. In order to prime the replacement cartridges, a 10mL slip tip syringe has to be inserted through the exit port of the cartridge while gently suctioning vehicle through the cartridge until liquid enters the syringe. It is important to first remove both rubber stoppers from the filling ports, otherwise no liquid will be suctioned (Fig. 3.1). After that, the Epson OEM cartridges must be removed and replaced by these aqueous vehicle filled replacement cartridges. Black, magenta, yellow, and cyan colored figures ought to be printed separately until the printing paper shows no trace of color. Series of solid block figures are recommended to be used to guarantee optimal cleaning results. Black pictures must be printed with the setting "black ink only option" selected in the print panel. At this point a new empty replacement cartridge is filled up with JS-B25P Metalon conductive ink. The use of a 10mL slip tip syringe is again recommended for the purpose of filling cartridges. It is also important to remove both of the rubber stoppers from the filling ports, then with the aid of the slip tip syringe the conductive ink is introduce in the cartridge. Following this, the cartridge must be primed as explained previously. The rubber stoppers

will then be put back into proper place and the black aqueous vehicle filled cartridge is replaced by the recently primed Metalon ink filled cartridge. As soon as the new cartridge is inserted, the printer will complete a head cleaning automatically. Head nozzle checks will print out lined patterns that will indicate the cleanliness of the nozzles. In the event they are all functioning and firing correctly, patterns will show solid and continuous lines. If this is not the case, head cleaning must be performed until such lines are observed. Users must aware that head cleaning might have to be performed more than once until nozzle check print outs are succesful.

Fig. 3.1: Priming of cartridges.

3.4.2 Printing Routine

The printing preferences must be set to “best photo” in the Quality Option panel, “matte paper-heavyweight” type in the Paper Options panel, and “gray scale” in the Paper and Quality Options panel. It is also necessary to uncheck the “high speed” option in the Paper and Quality Options panel. These settings ensure higher printing quality by printing designs at a proper rate and with an appropriate drop size. It is important to indicate that the Novele IJ-220 substrate has only one polymer treated inkjet-compatible side. Only this side is to be used for proper conductive ink printing (Fig. 3.2).

Fig. 3.2: Printing.

3.4.3 Post-Printing and Curing Routine

The Novele IJ-220 PET-based printed electronics substrate is engineered to facilitate low-temperature curing [29]. The curing should be performed as soon as possible after printing. Initially, this study experimented with two different curing techniques. First, the baking technique was implemented by using a conventional oven set to 100° Celsius (Fig. 3.3). Periods of 3-4 hours proved to be sufficient to cure and completely set the ink on the substrate (Fig. 3.4). This study also experimented with the air drying technique. Printouts were left to air dry for the space of 10 hours. Figures 3.4 and 3.5 show the results of using the baking and air drying techniques, respectively. As it can be observed the the baking technique showed a more uniform final result, it also presented better conductivity values than the air dried patch. Therefore, the baking technique was chosen as the most idoneous curing technique.

Fig. 3.3: Curing of antennas.

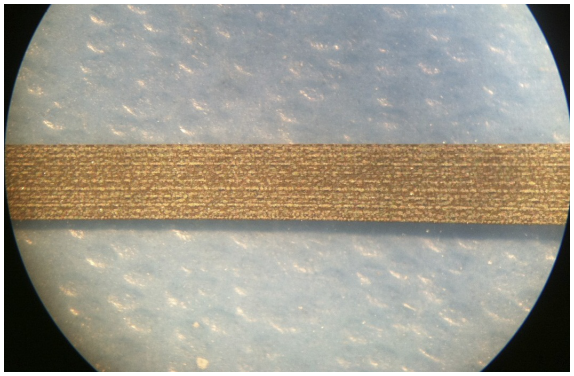

Fig. 3.4: Baked printout line.

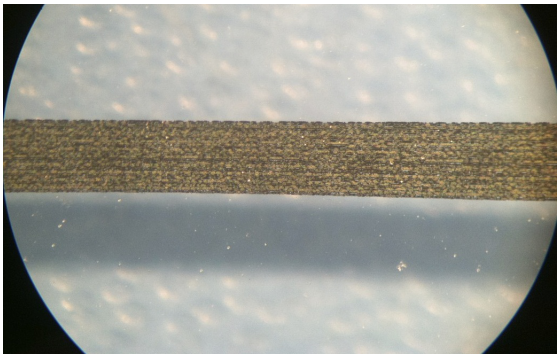

Fig. 3.5: Air dried printout line.

A thorough cleaning process will facilitate the proper functioning of the equipment in subsequent experiments; consequently, it must be considered as the last stage of the printing process. Immediately after the printing work is finished, the conductive ink filled cartridge must be removed and replaced with the black aqueous vehicle filled cartridge. Black solid block figures are to be printed until the printing paper shows no trace of color. Next, the printer's head and printer must be cleaned by, first, pushing the "replace ink cartridge" button on the printer to release the printer's head. This head must then be manually moved to the center of the carriage in order to clean any remaining ink on the printer's head. This must be done with the aid of a wet cleaning wipe or any other lint-free tissue (Fig. 3.6). In the same manner, the rubber squeegee and sponge on the right hand side of the carriage must be thoroughly cleaned. Finally, black solid figures are printed to ensure the lines have been completely flushed and the printer's head is completely clean.

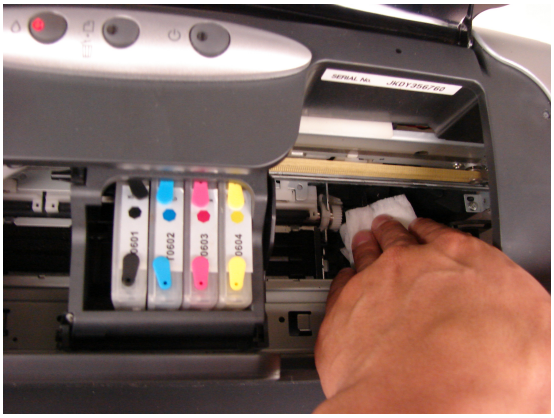

Fig. 3.6: Cleaning of printer.

Chapter 4

Extensive Measurements

In order to assess the feasibility of integrating highly transparent antennas with solar cells, a series of experiments were performed. These experiments were also aimed to understand the effect of solar cells on the antenna performance and the effect of meshed antennas on the efficiency of the solar cells.

4.1 Meshed and Solid Patch Antennas

Although the theory of meshed rectangular antennas has been presented in Chapter 2, in order to address the realistic feasibility and issues in practical fabrication using inkjet printing method, several antennas were printed, cured, and measured. A total of six meshed antennas with transparencies varying between 94.4% and 95% were measured. These meshed antennas were printed and cured at Novacentrix. In order to have a reference point a solid patch antenna was printed at USU using Metalon JS-B25P Silver conductive ink. All the meshed and solid antennas were printed on the same Novele IJ-220 films as described in Chapter 3.

The thickness of the ink on the film is between 500 nm and 700 nm, which is thinner compared to the skin depth at the operational frequency (refer to Section 4.3 for more detailed discussions on the skin depth). Therefore, for the solid patch printed at Utah State University, a layer of ink was manually brushed to increase the thickness of the metal layer. The process is as follows. First a solid patch antenna was printed with conductive ink. Then, the film with the solid antenna on it was baked in an oven for 4 hours. After curing it in the oven, a new layer of the same conductive ink was brushed on top of the solid patch and then baked in the oven for another 4 hours. The measured S11 and gain of solid (Measurement 1) and meshed antennas (Measurements 2-7) are listed in Table 4.1.

Also, the S11 parameters and radiation patterns for measurements 2, 3, and 5 are shown in Figures 4.1-4.6, respectively. These results draw conclusions about solid and meshed patches' performance.

Table 4.1: S11 and gain of meshed patch antennas on Rogers board.

Filename	S11	Frequency	Gain
measurement 1	-16.54 dB	2.67 Ghz	6.94 dB
measurement 2	-15.5 dB	2.47 Ghz	3.12 dB
measurement 3	-17.5 dB	2.47 Ghz	2.33 dB
measurement 4	-18.25 dB	2.39 Ghz	1.54 dB
measurement 5	-40.08 dB	2.44 Ghz	2.51 dB
measurement 6	-17.58 dB	2.38 Ghz	1.51 dB
measurement 7	-19.30 dB	2.42 Ghz	1.74 dB

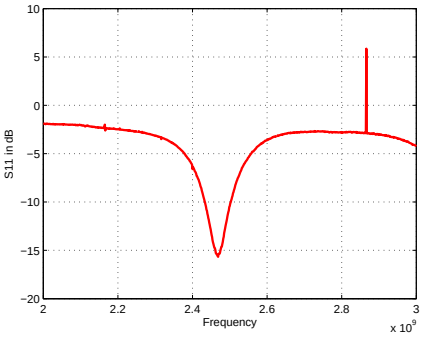

Fig. 4.1: S11 for measurement 2.

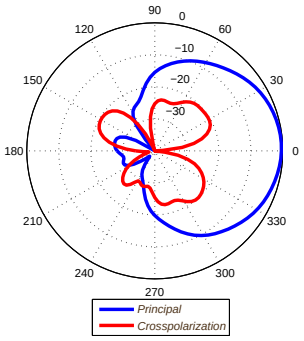

Fig. 4.2: E plane radiation pattern for measurement 2.

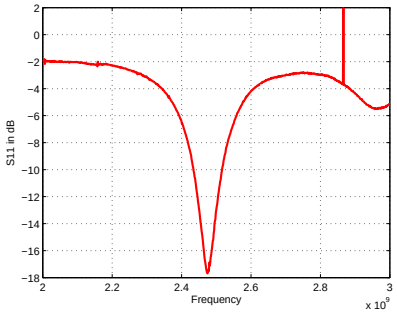

Fig. 4.3: S11 for measurement 3.

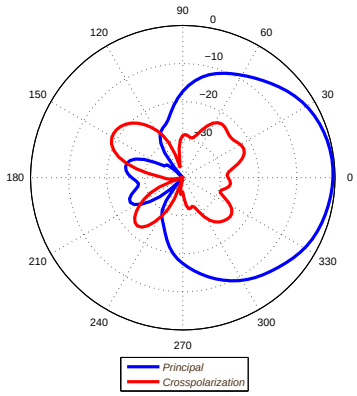

Fig. 4.4: E plane radiation pattern for measurement 3.

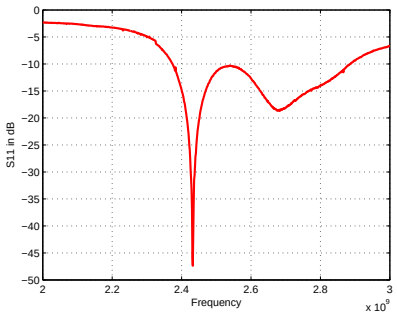

Fig. 4.5: S11 for measurement 5.

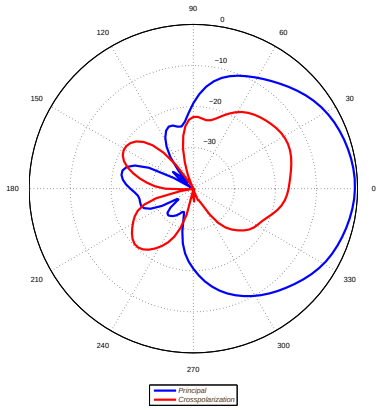

Fig. 4.6: E plane radiation pattern for measurement 5.

From Table 4.1, it is seen that the gain of the solid patch (after touchup) is close to the theoretical result of 7 dB. The average gain of the meshed antennas is 2.13 dB, which is lower than theoretical value of around or above 4.5 dB. This is clearly due to the very thin layer of the ink. As seen from Fig. 2.4, meshing a non-perfect conductor has more effect in gain reduction compared to a perfect conductor. Therefore, meshing a conductor that is thinner than the skin depth results in the reduced gain.

4.2 Orientation of the Antenna on Solar Cells

The CV-2500 controlled volatility Silicone is a two-part, optically clear silicone system especially designed for low-strength applications such as solar cell arrays. The present study experimented with a 10.2 cm wide, 8.9 cm long, and 1.005 mm thick piece of this material (Fig. 4.7). This silicone also has two rectangular solar cells attached to its surface which are 7.65 cm wide and 3.67 cm long. Due to the geometrical arrangement of the solar cells on the silicone, more than one physical set up is possible for the measurement of printed meshed patch antennas.

Even though there exist multiple ways the patch antennas can be placed on the silicone for testing purposes, this study considers two different setups in order to establish the most advantageous combination. The orientations are designated by the location of the feedline

in relation to the area located in between both solar cells. Figure 4.8 and figure 4.9 show the “perpendicular” and “parallel” arrangements, respectively.

Printed meshed patch antennas were constructed and measured with both orientations. These meshed patch antennas were printed and cured by Novacentrix Corp. Finally, in order to measure the gain levels of the above mentioned antennas, a 11 cm by 11 cm shielded Rogers board is used as the base support for the system. Both copper layers were left on the Rogers board and the edges were shielded (shorted) with pieces of copper tape. The Rogers board with shielded walls acts as the ground plane. The CV-2500 Silicone was placed on top of the shielded Rogers board. The meshed patch antenna was then placed on top of the silicone. The feed lines were soldered to the connectors. After this assembly, the film with the meshed patch and the feed line on it was taped down to the board with regular scotch tape as an attempt to remove the air in between layers.

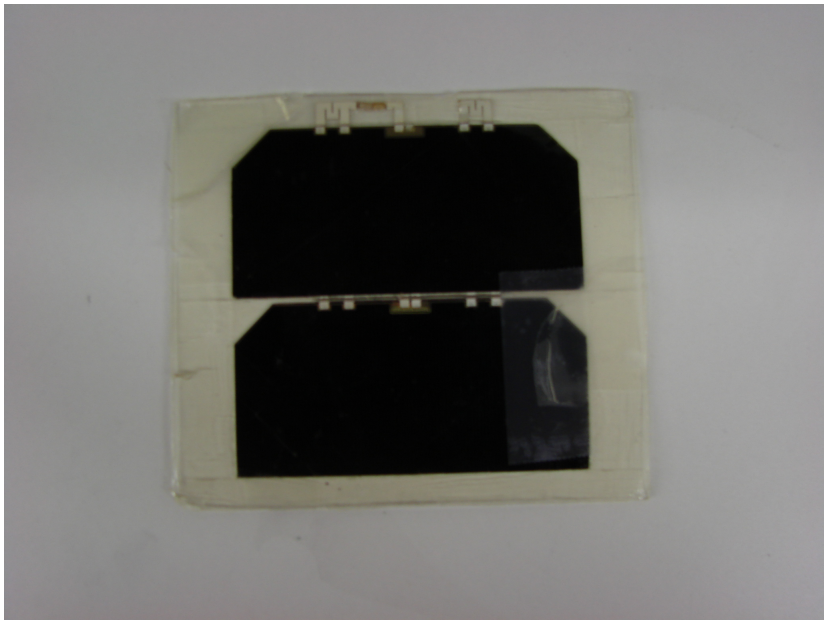

Fig. 4.7: CV-2500 controlled volatility silicone.

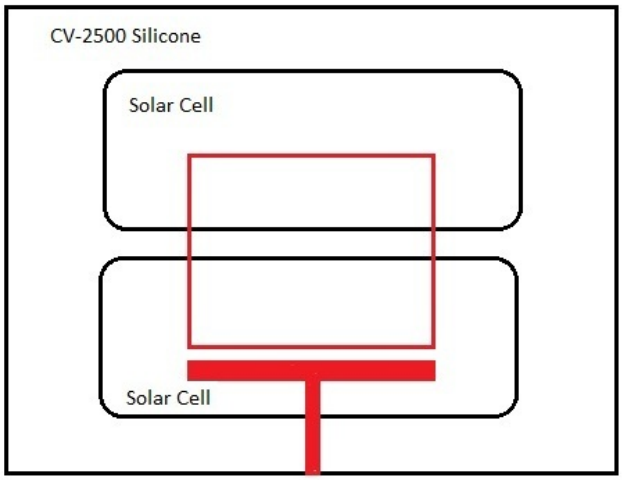

Fig. 4.8: Perpendicular orientation.

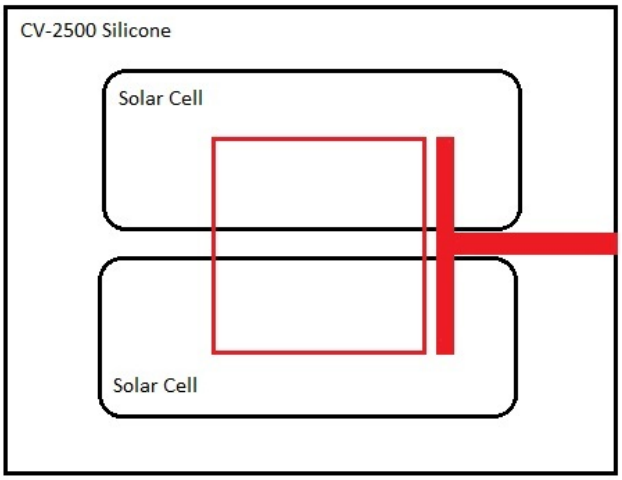

Fig. 4.9: Parallel orientation.

From the measurements in Tables 4.2 and 4.3, it is seen that the performance of the antennas in parallel and vertical orientations are mostly comparable. The gain (-0.53) in Table 4.2 may not be accurate, and therefore the test was repeated for another meshed antenna (with different lines) shown in Table 4.3. Although a significant difference of the antenna performance in the two assemblies was not observed, from S11 plots (Figs. 4.10, and 4.11 and Figs. 4.14 and 4.15), the perpendicular assembly shows slightly less loss. This seems reasonable because there may be some coupling between the feed line and the solar cells in the parallel orientation. Also, Figs. 4.12, 4.13, 4.16, and 4.17 show the radiation patterns of the parallel and vertical setups, respectively. It should be noted that the bottom layer of the solar cells are conductors and such a coupling may result in loss in antenna performance. Because of this reason, in the following studies, only the perpendicular orientation was considered.

Table 4.2: Measurement 8.

Orientation	Parallel	Vertical
Frequency	3.43 Ghz	3.48 Ghz
Gain	-0.53 dB	3.02 dB
S11	-13.6	-17.78
Crosspolarization	-25 dB	-27 dB
Number of vertical lines in mesh	11	11
Number of parallel lines in mesh	5	5

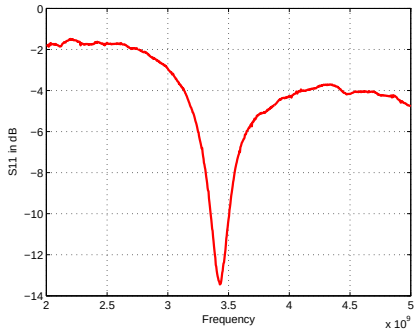

Fig. 4.10: S11 of parallel setup.

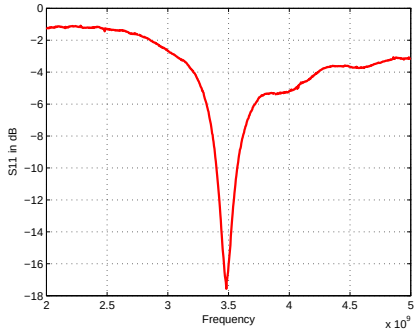

Fig. 4.11: S11 of vertical setup.

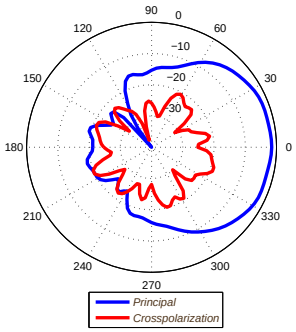

Fig. 4.12: E plane radiation pattern for parallel setup.

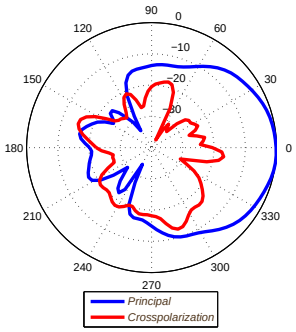

Fig. 4.13: E plane radiation pattern for vertical setup.

Table 4.3: Measurement 9.

Orientation	Parallel	Vertical
Frequency	3.63 Ghz	3.62 Ghz
Gain	2.19 dB	2.12 dB
S11	-25 dB	-25.8
Crosspolarization	-30 dB	-20 dB
Number of vertical lines in mesh	12	12
Number of parallel lines in mesh	5	5

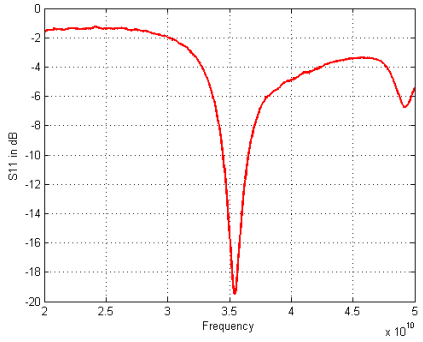

Fig. 4.14: S11 of parallel setup.

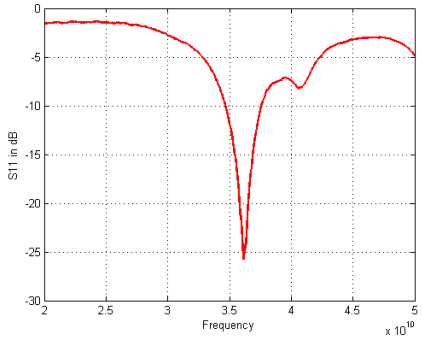

Fig. 4.15: S11 of vertical setup.

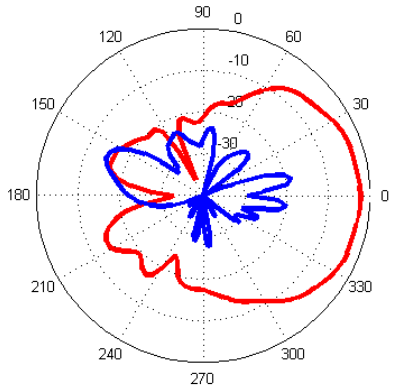

Fig. 4.16: E plane radiation pattern for parallel setup.

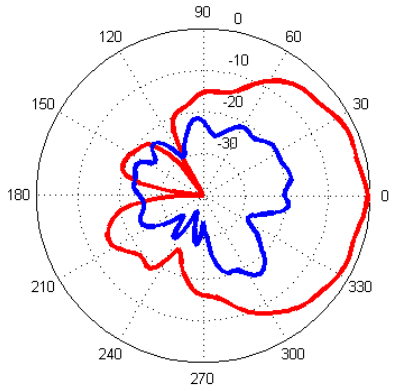

Fig. 4.17: E plane radiation pattern for vertical setup.

4.3 Effect of Solar Cells on Antenna Gain

The following tests were designed to estimate the effect of solar cells on the antenna performance. Before presenting the measured data, it is worthwhile to explain some terminologies used to describe the antenna geometry and assembly. It should be noted that all the meshed antennas in the following tests were printed and cured at Novacentrix, and all the solid patch antennas were printed and cured at USU.

Gel: Because the CV-2500 silicone substrates (with two solar cells embedded in it) has a gel-like texture, the substrate has been noted as "Gel" in the tests.

Shielded Gel: When the antennas were integrated on CV-2500 substrate, a metal backing was needed to serve as ground plane. For the ease of fabrication and soldering, instead of using a metal aluminum or copper plate, an original Rogers substrate was used (i.e. without printing any circuits on it, or without pealing copper layer on both sides) as the supporting layer for the CV-2500 silicone. In order to have the Rogers board serve as the ground plane, all four walls of the substrate were shorted using conductive copper tape. The assembly where antennas on CV-2500 substrate backed by a shielded Roger's board has been noted as "Shielded Gel."

Non-Shielded Gel: The assembly is similar to the "Shielded Gel" assembly except for the walls of the Rogers board were not shorted with copper tape. Also, the copper coating of the side that is contact with the Gel was removed.

Shielded Plastic: In order to assess the effect of the solar cells on the antenna's performance, it is essential to test antennas on the solar cell cover glass substrate without solar cell imbedded in it. The cover glass substrate is CV-2500 in this case. Due to the limited supply of CV-2500, a thermoplastic substrate with a close resemblance to CV-2500 was chosento perform the testing. This blue thermoplastic substrate is a copolyester plastic sheet called Vivak PETG. This substrate has a permittivity value of approximately 2.5 and a thickness of 0.97 mm. We note the assembly where a Vivak PETG plastic substrate is backed by a shielded Roger's board as "Shielded Plastic."

Non-Shielded Plastic: This assembly is similar to "Shielded Plastic" except for the walls

of the Rogers board were not shortened with copper tape. Also, the copper coating of the side that is in contact with the Gel was removed.

What follows (Tables 4.4-4.15 and Figs. 4.18-4.41) show the measured results, i.e. S11, resonance frequency, and gain values, in addition to presenting the S11 plot and radiation patterns for solid and meshed patches. It is important to notice that each section presents a different arrangement for the substrate.

Antennas on Shielded Gel:

Table 4.4: Measurement 10.

S11	-16.5 dB
Frequency	2.49 Ghz
Gain	-0.92 dB
Substrate	CV-2500 Silicone (solar cells) and shielded rogers
Crosspolarization	-40 dB

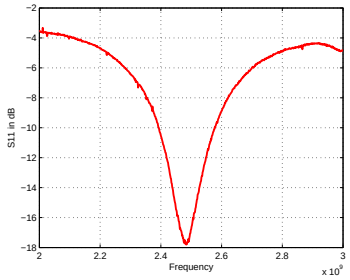

Fig. 4.18: S11 for shielded board - Measurement 10.

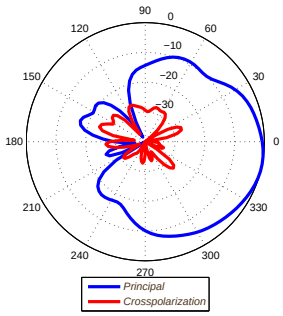

Fig. 4.19: E plane radiation pattern for vertical setup - Measurement 10.

Table 4.5: Measurement 11.

S11	-14.5 dB
Frequency	2.32 Ghz
Gain	-6.82 dB
Substrate	CV-2500 Silicone (solar cells) and shielded rogers
Crosspolarization	-25 dB
Number of vertical lines in mesh	12
Number of parallel lines in mesh	5

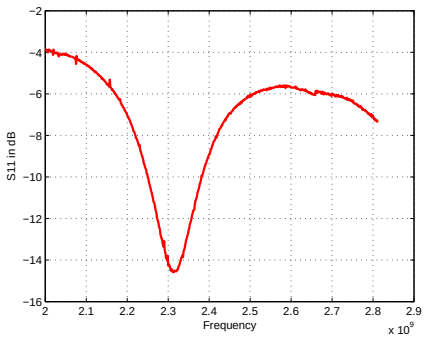

Fig. 4.20: S11 for shielded board - Measurement 11.

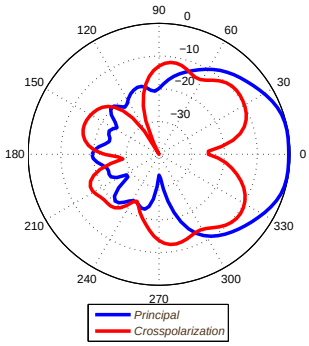

Fig. 4.21: E plane radiation pattern for vertical setup - Measurement 11.

Table 4.6: Measurement 12.

S11	-19.71 dB
Frequency	2.44 Ghz
Gain	-4.36 dB
Substrate	CV-2500 Silicone (solar cells) and shielded rogers
Crosspolarization	-40 dB
Number of vertical lines in mesh	14
Number of parallel lines in mesh	5

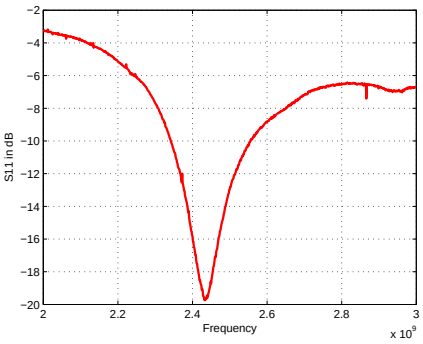

Fig. 4.22: S11 for shielded board - Measurement 12.

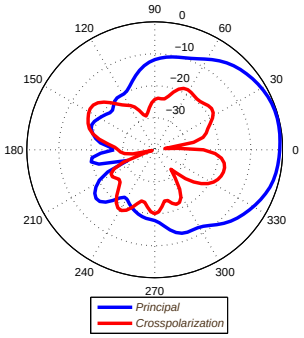

Fig. 4.23: E plane radiation pattern for vertical setup - Measurement 12.

Antennas on Unshielded Gel:

Table 4.7: Measurement 13.

S11	-13 dB
Frequency	2.51 Ghz
Gain	-2.61 dB
Substrate	CV-2500 Silicone (solar cells) and unshielded rogers
Crosspolarization	-34 dB
Number of vertical lines in mesh	11
Number of parallel lines in mesh	5

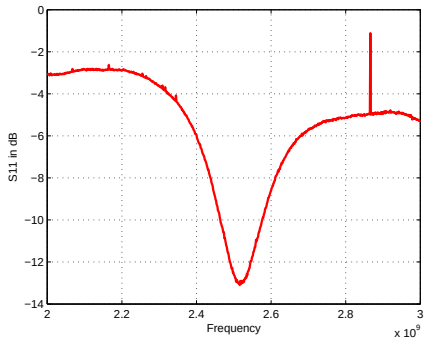

Fig. 4.24: S11 for unshielded board - Measurement 13.

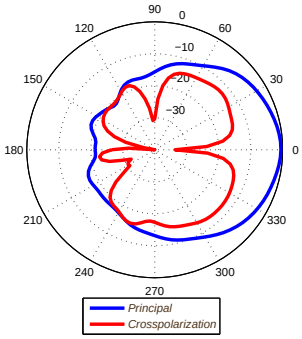

Fig. 4.25: E plane radiation pattern for vertical setup - Measurement 13.

Table 4.8: Measurement 14.

S11	-32.215dB
Frequency	3.095 Ghz
Gain	-1.57 dB
Substrate	CV-2500 Silicone (solar cells) and unshielded rogers
Crosspolarization	-22 dB
Number of vertical lines in mesh	14
Number of parallel lines in mesh	5

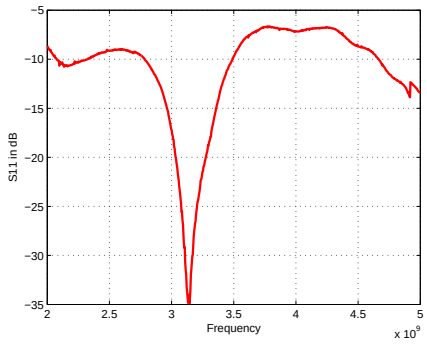

Fig. 4.26: S11 for unshielded board - Measurement 14.

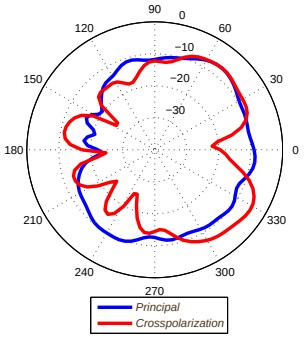

Fig. 4.27: E plane radiation pattern for vertical setup - Measurement 14.

Antennas on Shielded Blue Plastic:

Table 4.9: Measurement 15.

S11	-18.73 dB
Frequency	2.72 Ghz
Gain	3.28 dB
Substrate	Vivak PETG and shielded rogers
Crosspolarization	dB

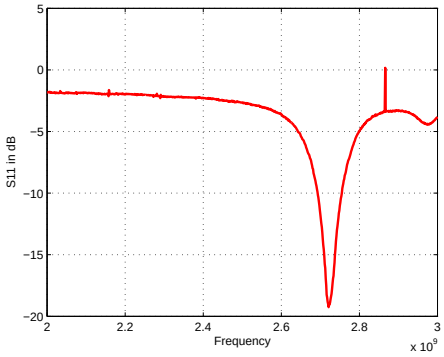

Fig. 4.28: S11 for shielded board - Measurement 15.

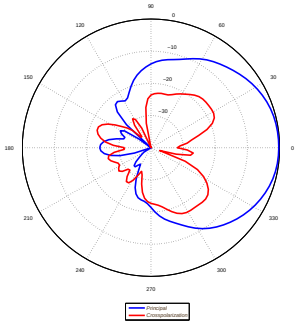

Fig. 4.29: E plane radiation pattern for vertical setup - Measurement 15.

Table 4.10: Measurement 16.

S11	-15.3 dB
Frequency	2.51 Ghz
Gain	-0.16 dB
Substrate	Vivak PETG and shielded rogers
Crosspolarization	-31 dB
Number of vertical lines in mesh	12
Number of parallel lines in mesh	5

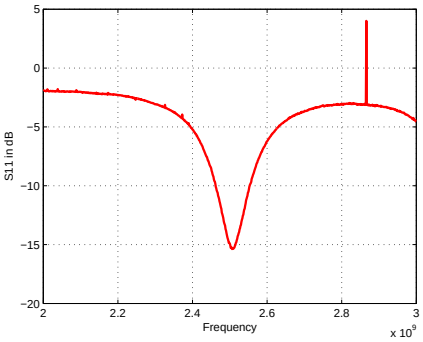

Fig. 4.30: S11 for shielded board - Measurement 16.

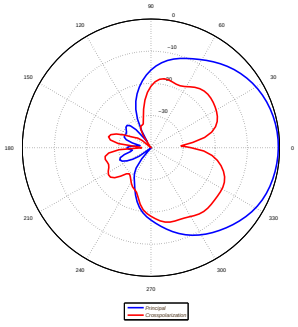

Fig. 4.31: E plane radiation pattern for vertical setup - Measurement 16.

Table 4.11: Measurement 17.

S11	-18.45 dB
Frequency	2.59 Ghz
Gain	-3.59 dB
Substrate	Vivak PETG and shielded rogers
Crosspolarization	-25 dB
Number of vertical lines in mesh	14
Number of parallel lines in mesh	5

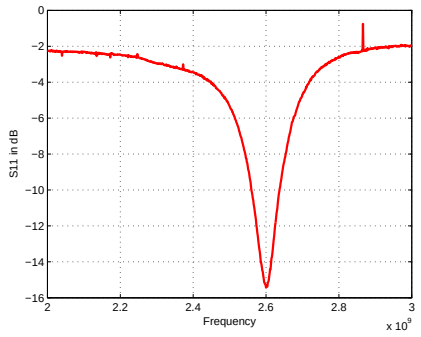

Fig. 4.32: S11 for shielded board - Measurement 17.

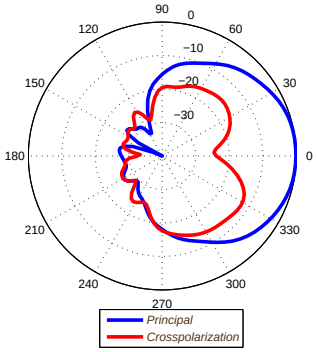

Fig. 4.33: E plane radiation pattern for vertical setup - Measurement 17.

Antennas on Unshielded Blue Plastic:

Table 4.12: Measurement 18.

S11	-22 dB
Frequency	2.34 Ghz
Gain	5.44 dB
Substrate	Vivak PETG and shielded rogers
Crosspolarization	-40 dB

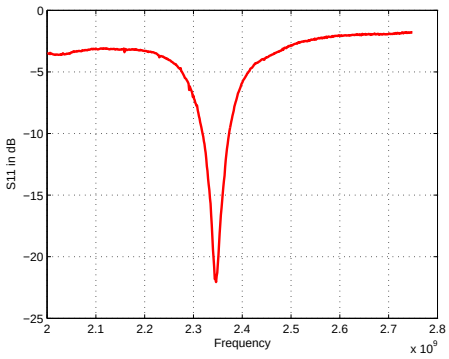

Fig. 4.34: S11 for shielded board - Measurement 18.

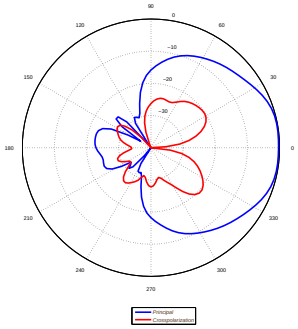

Fig. 4.35: E plane radiation pattern for vertical setup - Measurement 18.

Table 4.13: Measurement 19.

S11	-15.11 dB
Frequency	2.39 Ghz
Gain	4.44 dB
Substrate	Vivak PETG and unshielded rogers
Crosspolarization	-32 dB
Number of vertical lines in mesh	14
Number of parallel lines in mesh	5

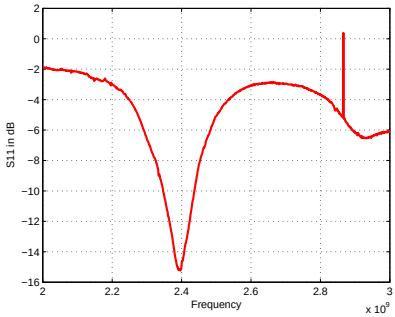

Fig. 4.36: S11 for unshielded board - Measurement 19.

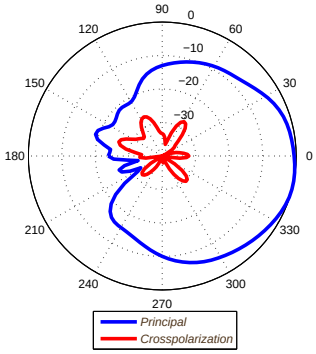

Fig. 4.37: E plane radiation pattern for vertical setup - Measurement 19.

Table 4.14: Measurement 20.

S11	-14.64 dB
Frequency	2.43 Ghz
Gain	4.96 dB
Substrate	Vivak PETG and unshielded rogers
Crosspolarization	-40 dB
Number of vertical lines in mesh	14
Number of parallel lines in mesh	5

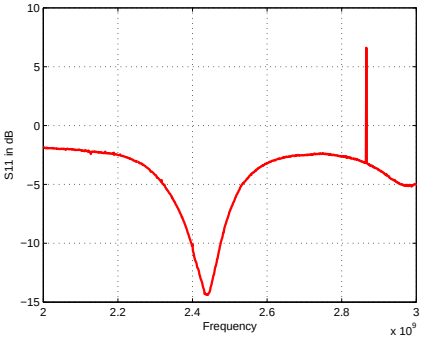

Fig. 4.38: S11 for unshielded board - Measurement 20.

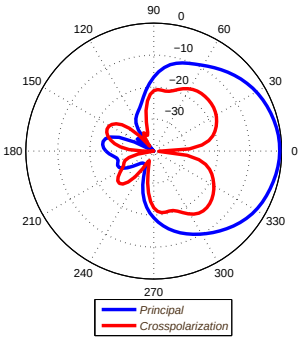

Fig. 4.39: E plane radiation pattern for vertical setup - Measurement 20.

Table 4.15: Measurement 21.

S11	-13.1 dB
Frequency	2.7 Ghz
Gain	1.42 dB
Substrate	Vivak PETG and unshielded rogers
Crosspolarization	-25 dB
Number of vertical lines in mesh	12
Number of parallel lines in mesh	5

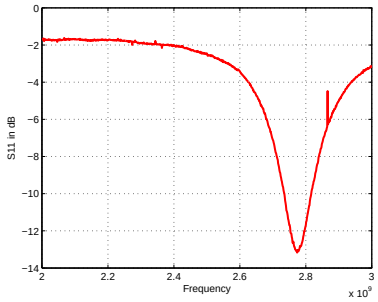

Fig. 4.40: S11 for unshielded board - Measurement 21.

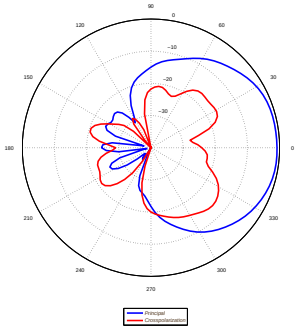

Fig. 4.41: E plane radiation pattern for vertical setup - Measurement 21.

Summary on the Effect of Solar Cells: The previous section presented extensive measurements of different antennas (solid and transparent) on solar cell or cover glass material. When estimating the effect of solar cells, it is easier to list all of related measurements. Therefore, those measurements that are used to calculate the effect of solar cells are listed in Table 4.16. The effect of solar cells is calculated by using the gain of an antenna on the cover glass material (designated as plastic) minus the gain of the same antenna over solar panel (designated as gel). The calculated gain difference is listed in Table 4.17. As it can be seen, the antenna was not measured (with the line number of 12 x 5) on un-shielded gel. Instead, the measurement was performed on a 13 x 5 mesh due to the resources at the time of the experiment. But the difference between a 13 x 5 mesh and 12 x 5 mesh is only a 0.15 mm line. Therefore, the gain of the 12 x 5 mesh on unshielded gel was approximated with the one for 13 x 5 mesh. Hence, these results were designated with an approximate sign of $\approx$ in Table 4.17. As it can be observed, the difference in gain is fairly not conclusive. But after taking an average, it shows about 4.3 dB difference at around 2.5 GHz. Another observation is that the gain of the 14 x 5 mesh on shielded plastic is low. The gain should be higher than the 12 x 5 mesh on the same set up. Therefore, as an adjustment, the gain of the 14 x 5 mesh on the shielded plastic was approximated to 0 dB. With this adjustment, the average gain difference is calculated to be 4.9 dB. The measured effect of the solar cell is high (close to 5 dB), which may evidence no practical use for the implementation of integrating antennas with solar cells when the cells exhibit such a high loss. But, this experimental set-up has been very much "lossy" at the present time. The assembly consists of copper tape and scotch tape. The printing may not be consistent for the same mesh when printed multiple times. Also, there exist two pieces of solar cells imbedded in gel material used in the experiments. Towards the end of this study, the cells were fairly broken. Therefore, the effect of the solar cells was expected to be lower than the current results with improvement measurements. In addition to these results, when the frequencies are raised, the solar cell layer may act mainly like a ground, and less loss due to the solar cells were expected for frequencies higher than S band.

Table 4.16: S11 and gain of meshed patch antennas on plastic and gel.

Filename	Gain	Description	Number of Lines
Measurement 17	-3.59 dB	plastic on shielded Rogers	14 by 5
Measurement 19	4.44 dB	plastic on unshielded Rogers	14 by 5
Measurement 20	4.96 dB	plastic on unshielded Rogers	14 by 5
Average of previous two	4.7 dB	plastic on unshielded Rogers	14 by 5
Measurement 12	-4.36 dB	gel on shielded Rogers	14 by 5
Measurement 14	-1.57 dB	gel on unshielded Rogers	14 by 5
Measurement 13	-2.61 dB	gel on unshielded Rogers	13 by 5
Measurement 11	-6.82 dB	gel on shielded Rogers	12 by 5
Measurement 21	1.42 dB	plastic on unshielded Rogers	12 by 5
Measurement 16	-0.16 dB	plastic on shielded Rogers	12 by 5
Measurement 18	5.44 dB	plastic on unshielded Rogers	Solid patch
Measurement 15	3.28 dB	plastic on shielded Rogers	Solid patch
Measurement 10A	-0.66 dB	gel on shielded Rogers	Solid patch-Horizontal
Measurement 10	-0.915 dB	gel on shielded Rogers	Solid patch-Vertical

Table 4.17: Gain difference for antennas on plastic and gel.

Antennas	Gain Difference	Adjusted
14 by 5 shielded	0.768 dB	4.358 dB
14 by 5 unshielded	6.2725 dB	6.2725 dB
12 by 5 unshielded	6.661 dB	6.661 dB
12 by 5 $\approx$ unshielded	4.028 dB	4.028 dB
Solid Shielded H	3.936 dB	3.936 dB
Solid Shielded V	4.191 dB	4.191 dB
Average	4.309 dB	4.907 dB

4.4 Discussions on Gain Enhancement

From the measured results in Section 4.3, it is seen that the gain of the antenna on solar cell is generally low. This low gain is mainly due to three reasons: Reason 1, loss due to the solar cell; Reason 2, loss due to the assembly (such as air in between layers, use of copper tape and scotch tape, imperfect soldering, etc.); Reason 3, very thin cover glass. It is well known that a very thin substrate results in a low gain patch antenna [18]. In order to achieve a higher gain, the frequency may be increased, or a thicker cover glass may be used. While there is limited freedom in choosing the thickness of solar cell cover

glass, an alternative method is to find ways to "thicken" the substrate. In practice, for a CubeSat panel, there is some space between solar cells for connections. Also, solar cells are not laid exactly from the edge of the solar panel, and there is some space between the edge of cover glass and solar cell. So, when a secondary substrate is placed under the solar cell, due to the coupling through these spaces, the substrate for the antenna (on top of the cover glass) seems to be thicker than the cover glass. Accordingly, one expects gain improvement. It should be mentioned that most CubeSats use circuit board material as the solar panel material. Therefore, using a circuit board material to "thicken" the substrate for antennas is practical. This assumption has been proven through experiments as shown in Table 4.16, where the average gain improvement from "shielded gel" assembly to "unshielded gel" is more than 3 dB. Of course, such an enhancement is based on the "spacing" between solar cells. If on some solar panel, the cells are placed very tight, and if there is no gap between solar cell and the boundary of the solar panel, then such an enhancement method may not be useful.

4.5 Discussions on Skin Depth

It is well understood that the thickness of the patch material needs to be larger than the skin depth. For a normal conductor, the skin depth can be computed from

$$\delta_s = \frac{1}{\pi f \mu_o \delta}, \tag{4.1}$$

where f is the frequency, δ is the RF conductivity, and μ_o is the free space permeability. For the conductive ink, after curing, the conductivity is good enough to consider the printed sheet as a good conductor, but not as high as a copper sheet. Therefore, we represent the conductivity of the ink layer with

$$\delta = \delta_c k_{def}, \tag{4.2}$$

where δ_c is the conductivity of copper, and k_{def} is a defection factor that represents the how well the conductive ink behaves as a conductor. For example, when $k_{def} = 1$ it means the

printed conducive sheet is virtually the same as a copper sheet. When $k_{def} = \frac{1}{100}$, it means the lines or area printed from conductive ink is 100 times less conductive than fabricated from copper. Using (4.1) and (4.2), the skin depth for a patch printed was calculated by conductive ink for various k_{def} values (Table 4.18). The operational frequency is around 3 Ghz.

Table 4.18: Calculated skin depth.

Frequency (Ghz)	Defection Factor(k_{def})	Skin Depth (m)
3	0.1	3.6910^{-6}
3	0.01	1.1710^{-5}
3	0.001	3.6910^{-5}
3	0.0001	1.1710^{-4}
5	0.1	2.8610^{-6}
5	0.01	9.0410^{-6}
5	0.001	2.8610^{-5}
5	0.0001	9.0410^{-5}
10	0.1	2.0210^{-6}
10	0.01	6.3910^{-6}
10	0.001	2.0210^{-5}
10	0.0001	6.3910^{-5}
50	0.1	9.0310^{-7}
50	0.01	2.8610^{-6}
50	0.001	9.0310^{-6}
50	0.0001	2.8610^{-5}
170	0.1	4.9010^{-7}
170	0.01	1.5510^{-6}
170	0.001	4.9010^{-6}
170	0.0001	1.5510^{-5}

The thickness of the ink from the commercial printer used is around 500-700 nm. Therefore, from Table 4.18, it is seen that this thickness is thinner than the skin depth even for $k_{def} = 1$. Therefore, it can be concluded that there exists a relative high loss in our printed antennas due to the very thin ink layer. To access the claim that this printed antenna exhibits high loss because the ink layer is thin, two experiments were designed as follows.

First, a solid patch antenna was printed and assembled on "unshielded plastic." The Rogers material is RO 4003C high frequency laminate. It has a permittivity value of 3.38

and a thickness equal to 0.813 mm [16]. The antenna operates at 2.98 GHz. Without doing any touch up, the antenna is measured and showed a gain of 4.469 dB. Then, the patch antenna is brushed with conductive ink to increase the thickness of the layer and then sent to the oven for 4 hours at 100° Celsius. The gain of the patch antenna with touch up and same assembly is measured and found to be 7.172, which is close to theoretical value. The experiment confirms that the thickness of the ink plays an important role in the antennas' performance. Finally, a simple test was performed to assess the value for k_{def}. A thick line was fabricated (like a microstrip line) with a copper tape on a PET substrate, the resistance of the line was measured for a given distance (9 mm) using a multi-meter. The same line was then printed on the same substrate using conductive ink. After the ink was cured, the resistance was measured for the same distance as for the copper tape. The resistance of the copper was used to divide the value for the conductive ink to get k_{def}. Using this simple method, these experiments showed k_{def} approximately to be $\frac{1}{188}$. Referencing to Table 4.18, this k_{def} value means the thickness of the ink should be at least 490 nm at 170 GHz. The thickness of the ink experimented by at Georgia Tech. University is 12 μm [30], which is larger than the skin depth. New methods to improve the thickness of the printed the structure need to be investigated.

4.6 Effect of the Transparent Antennas on Solar Cell Performance

The effect of the 95% transparent antenna on the performance of solar cells was measured at the facilities at the Space Dynamics Laboratory (SDL). The set-up is as follows. A meshed patch with 95% transparency printed on a PET film is placed on a 4-cell solar panel, and then the solar panel is illuminated by an artificial light bulb array (Fig. 4.42). The standard I-V curve of the solar panel is measured to calculate its efficiency. The solar cells are all triple junction space certified cells. Comparative measurements were performed to assess the effect of meshed antennas on solar cells. I-V curves of solar cells were measured by covering the solar panel without been covered by object, covered with blank PET film, and covered with a PET film that has a 95% meshed antenna (without the feed line) printed on it. It is concluded that for a two-cell solar panel (usually the case for a cube satellite),

the overall effect of the antennas on the solar panel is less than 3%, which is comparable to the shadow cast by a traditional wire antenna used on cube satellites.

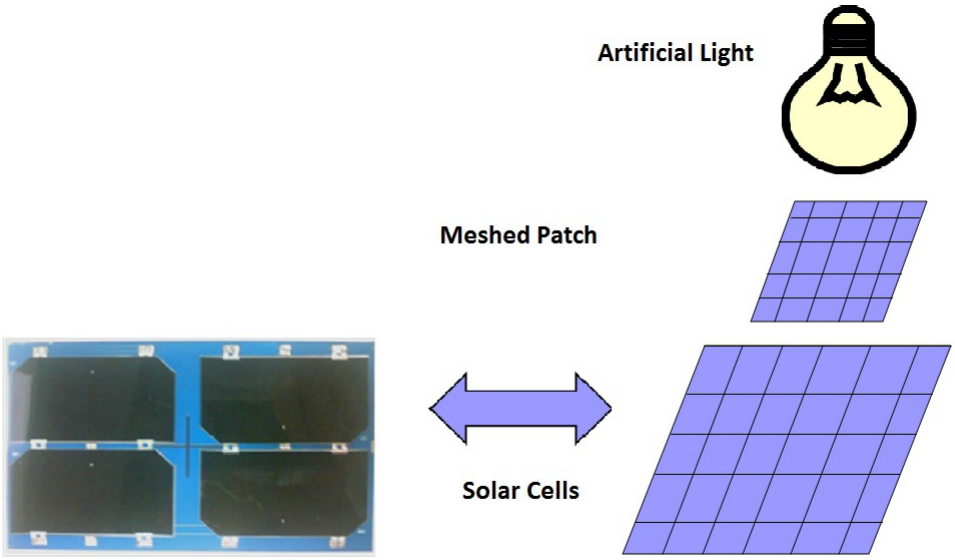

Fig. 4.42: SDL setup.

Chapter 5

Conclusions

The purpose of this thesis is to study the integration of highly transparent meshed antenna with solar cells. In order to integrate antennas on solar cells, one has to design and prototype the antenna first. Accordingly, this thesis explores different prototyping methods to achieve highly transparent and effective meshed patch antennas. Considering the trade-offs between three fabrication schemes (electroformation, screen printing and inkjet printing), inkjet printing method has been chosen to be the prototyping method. The inkjet printing method is extremely inexpensive because only conductive ink (Nanosilver aqueous dispersive ink Metalon JS-B25P), receptive PET film (Novele IJ-220), and a commercial inkjet printer (less than $100.00) are needed. The printing routine and curing techniques are discussed in detail in this thesis. After achieving highly transparent ($\geq$ 95%) antennas, the next task is to integrate them on top of triple junction space-certified solar cells. There are two main objectives in initial integration: (1) to assess the effect of solar cells on the antenna's performance, and (2) to assess the effect of the antennas on solar cell's performance. To achieve the first objective, several different antennas (solid non-transparent patches and meshed transparent patches) were tested on substrates (solar cell cover glass) with and without solar cells imbedded. By examining the difference between the two tests (with and without solar cells), it is assessed that the solar cells may result in about 5 dB gain reduction on the antenna performance. This number is high in order to consider such integration in practical application. However, there have been a few assembly and printing imperfections that may affect the test results. One may be able to reduce such loss to 3 dB with more accurate assembly and test procedure. On the other hand, the operational frequency in this thesis study is in S-band. When the operational frequency is increased, one may expect lower loss due to solar cell because solar cell may be approximated as part of

the ground in that case. To achieve the second objective, a meshed patch antenna with 95% transparency and without the feed-line is placed on an active solar panel. The efficiency of the solar panel was then measured using standard procedure at SDL (Space Dynamics Laboratory, Logan UT). It has been concluded that for a two-cell solar panel, the reduction of the solar cell efficiency due to a 95% meshed antenna integrated on top of them is less than 3%. It should be noted that the shadow cast by dipole antennas on solar panel is about 3%, and therefore, integrating 95% transparent antenna on solar cells does not yield additional efficiency decrease compared to today's dipole antennas used in cube satellites. This thesis has also studied the effectiveness of inkjet printing in terms of skin depth. The ink layer is very thin and thinner than the skin depth in most cases, and therefore, the antennas printed show reduced gain compared to theoretical results. This may have been another "loss" factor in the test assembly. Possible improvement includes choosing a more advanced printer or printing the antenna structure multiple times to ensure a thick layer of ink. Finally, it is concluded that most commonly used solar cell cover glass is too thin for an antenna to be effective. In order to have antenna with a gain more than 0 dB, either a thicker cover glass is needed or one has to raise the operational frequency. When a thicker cover glass may not be practical, it has been shown that one may manually "thicken" or "enhance" the antenna substrate by adding a circuit board substrate beneath the solar cells. Such an enhancement is based on the fact that there are some spaces between solar cells and therefore the coupling between antenna, cover glass, and circuit board produces a "thicker" substrate. In conclusion, if the loss on solar cell can be reduced to less than 2 dB (for S band or higher frequency), and the assembly loss to 0.5 dB, then it is feasible to have more than 2 dB gain for a 95% transparent mesh on an enhanced substrate.

References

[1] R. N. Simons and R. Q. Lee, "Feasibility study of optically transparent microstrip patch antenna," in *NASA Lewis Research Center Memorandum 107434*.

[2] T. Turpin and R. Baktur, "Meshed patch antennas integrated on solar cells," *IEEE Antennas and Wireless Propagation Letters*, vol. 8, pp. 693–696, 2009.

[3] S. Vaccaro, P. Torres, J. R. Mosig, A. Shah, J. Zurcher, A. K. Skivervik, F. Gardiol, P. de Maagt, and L. Gerlach, "Integrated solar panel antennas," *Electronic Letters*, vol. 36, pp. 390–391, 2000.

[4] S. Vaccaro1, P. Torres, J. R. Mosig, A. Shah, J. Zurcher, A. K. Skivervik, F. Gardiol, P. de Maagt, and L. Gerlach, "Stainless steel slot antennas with integrated solar cells," *Electronic Letters*, vol. 36, pp. 2059–2060, 2000.

[5] A. Porch, D. V. Morgan, R. Perks, M. Jones, and P. P. Edwards, "Electromagnetic absorption in transparent conducting films," *Journal of Applied Physics*, vol. 95, p. 4734, 2004.

[6] N. Guan, H. Furuya, D. Delaune, and K. Ito, "Antennas made of transparent conductive films," in *Progress in Electromagnetics Research Symposium proceedings*, 2008.

[7] N. Outaleb, J. Pinel, M. Drissi, and O. Bonnaud, "Microwave planar antenna with rf-sputtered indium tin oxide," *Microwave and Optical Tecnology Letters*, vol. 24, 2000.

[8] J. Saberin and C. Furse, "Challenges with optically transparent patch antennas for small satellites," in *Antennas and Propagation and URSI (Union Radio-Scientifique Internationale) proceedings*, 2010.

[9] K. Oshima, N. Kidera, K. Niwano, K. Ikawa, R. Sonoda, and S. Kawasaki, "Use of a transparent conductive thin-film on a glass substrate in active integrated antenna array with double strong coupling," in *Proceedings IEEE MTT-S Dig.*, 2002.

[10] M.-S. Wu and K. Ito, "Basic study on see-through microstrip antennas constructed on a window glass," in *Proceedings IEEE AP-S International Symposium*, 1992.

[11] G. Clasen and R. Langley, "Meshed patch antennas integrated into car windscreen," *Electronic Letters*, vol. 36, pp. 781–782, 2000.

[12] G. Clasen1 and R. Langley, "Meshed patch antennas," *IEEE Transactions on Antennas and Propagation*, vol. 52, pp. 1412–1416, 2004.

[13] G. Clasen2 and R. Langley, "Gridded circular patch antennas," *Microwave and Optical Technology Letters*, vol. 21, pp. 311–313, 1999.

[14] J. James and P. Hall, *Handbook of Microstrip Antennas*. London, UK: Peter Peregrinus Ltd., 1989.

[15] S. Vaccaro, J. R. Mosig, and P. de Maagt, "Two advanced solar antenna 'solant' designs for satellite and terrestrial communications," *Transactions on Antennas and Propagation*, vol. 51, pp. 2028–2034, 2003.

[16] Rogers Corp., "Ro 4000 series high frequency circuit materials," [www.rogerscorp.com], 2011.

[17] Nusil Silicone Technology, "Cv10-2500 controlled volatility silicone - product profile," [www.nusil.com], 2011.

[18] R. Bancroft, *Microstrip and Printed Antenna Design.* Raleigh: SciTech Publishing Inc., 2009.

[19] H. Eskelinen and P. Eskelinen, *Microwave Component Mechanics.* Norwood: Artech House Inc., 2003.

[20] M. Lambrechts and Sansen, *Biosensors: Microelectrical Devices.* Philadelphia: Institute of Physics Publishing, 1992.

[21] E. Tekin, P. J. Smith, and U. S. Schubert, "Inkjet printing as a deposition and patterning took for polymers and inorganic particles," *Sort Matter*, vol. 4, pp. 703–713, 2008.

[22] D. Pesach and A. Marmur, "Marangoni effects in the spreading of liquid mixtures on a solid," *Langmuir*, vol. 3, pp. 519–524, 1987.

[23] J. Perelaer, P. J. Smith, M. M. P. Wijnen, E. V. de Bosch, S. S. C. V. Grootel, P. H. J. M. Ketelaars, and U. S. Schubert, "The spreading of inkjet-printed droplets with varying polymer molar mass on a dry solid substrate," *Macromolecular Chemistry and Physics*, vol. 210, p. 495, 2009.

[24] J. Perelaer1, P. J. Smith, M. M. P. Wijnen, E. V. de Bosch, S. S. C. V. Grootel, P. H. J. M. Ketelaars, and U. S. Schubert, "Droplet tailoring using evaporative inkjet printing," *Macromolecular Chemistry and Physics*, vol. 210, p. 387, 2009.

[25] M. Singh, H. M. Haverinen, P. Dhagat, and G. E. Jabbour, "Inkjet printing-process and its applications," *Advance Materials*, vol. 22, pp. 673–685, 2010.

[26] J. Mujal, E. Ramon, E. Daz, J. Carrabina, A. Calleja, R. Martnez, and L. Teres, "Inkjet printer antennas for nfc systems," in *Electronics, Circuits, and Systems (ICECS),17th IEEE International Conference*, 2010.

[27] Epson Corp., "Innovation," [http://global.epson.com/innovation/micro_piezo/ technology/], 2011.

[28] Novacentrix Corp., "Metalon, conductive inks for printed electronics-metalon js-b25p," [www.novacentrix.com], 2011.

[29] Novacentrix Corp.1, "Tools and materials for printed electronics novele ij-220," [www.novacentrix.com], 2011.

[30] R. Vyas, V. Lakafosis, A. Rida, N. Chaisilwattana, S. Travis, J. Pan, and M. Tentzeris, "Paper-based rfid-enabled wireless platforms for sensing applications," *IEEE Transactions on Microwave Theory and Techniques*, vol. 57, pp. 1370–1382, 2009.